

1 The effect of meteoric phreatic diagenesis and spring sapping on the formation of submarine collapse
2 structures in the Biak Basin, Eastern Indonesia

3 David P. Gold^{a,*}

4

5 ^{a,*} *SE Asia Research Group, Department of Earth Sciences, Royal Holloway University of London, Egham,*
6 *Surrey, TW20 0EX, United Kingdom*

7

8

9 This article has been submitted for publication and will appear in a revised form in *Geomorphology*.

10 Please carefully note that subsequent versions of this manuscript may have different content

* Corresponding author at: Department of Earth Sciences, Royal Holloway University of London, Egham, Surrey, TW20 0EX, United Kingdom. Tel: +44 1784 443897

E-Mail address: david.patrick.gold@gmail.com (David Gold)

11 **ABSTRACT**

12 The islands of Biak and Supiori, situated in the Bird's Head region of New Guinea, comprise
13 predominantly Neogene age carbonate units that extend offshore into the adjacent Biak Basin. Unusual
14 geomorphologic features including pockmarks, headless canyons and semi-circular collapse structures
15 identified in multibeam bathymetric imagery occur on the southern margin of the Biak Basin. These
16 features have a bathymetric expression distinct from strike-slip faults of the Biak Fault Zone which
17 bound the eastern margin of the basin. The Biak Fault Zone comprises several seismically active,
18 segmented and parallel fault strands. Seismicity along the Biak Fault Zone is responsible for the
19 shedding of mass transport deposits into the basin, however these are absent from the geomorphologic
20 features along the southern margin of the basin. Instead, these features appear isolated and unrelated to
21 activity of the Biak Fault Zone and are interpreted to have formed as a result of 'spring sapping' by
22 submarine aquifers. Rapid uplift during the Pliocene caused exposure and karstification of carbonates
23 from onshore Biak which extend into the offshore Biak Basin, providing conduits for a freshwater lens
24 to develop within older Miocene strata. Diagenetic cement textures and fabrics indicate that many
25 Miocene carbonates were subjected to meteoric diagenesis within freshwater aquifers that overprinted
26 burial cements. This is supported by stable isotope analyses of diagenetic cements which record
27 negative $\delta^{18}\text{O}$ values.

28

29

30

31

32

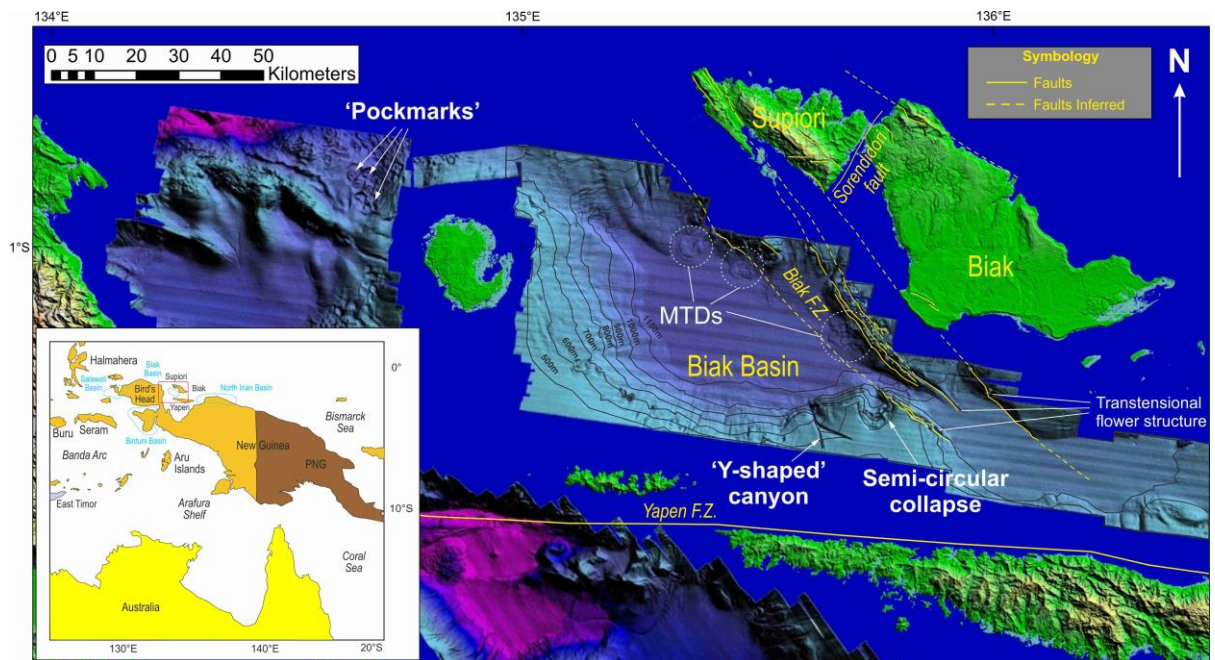
33

34 *Keywords:* Spring sapping, meteoric diagenesis, carbonates, aquifer

35

36 **1. Introduction**

37 The islands of Biak and Supiori are situated in the Indonesian province of Papua on the Pacific
38 island of New Guinea (Fig. 1). These islands form part of a small archipelago of islands north of
39 Cenderawasih Bay, a large embayment to the west of New Guinea (Fig. 1). Biak is the largest island
40 within this archipelago, with the island of Supiori located to the northwest (Fig. 1). The islands of Biak
41 and Supiori are separated by the Sorendidori Fault (Fig. 1), an oblique normal fault that downthrows
42 younger Neogene sediments of the island of Biak to the SE from Early to Middle Miocene carbonates
43 of the island of Supiori to the NW (Gold et al., 2017). Neogene sediments from Biak and Supiori are
44 predominantly carbonates that extend SW into the offshore Biak Basin, which is situated south of Biak
45 and Supiori, and north of Yapen Island (Fig. 1). The Biak Basin is bounded on its eastern margin by
46 the Biak Fault Zone, a series of parallel, NW-SE trending strike-slip faults that form the linear west
47 coast of Supiori and Biak (Gold et al., 2017; Fig. 1). These faults also form clearly expressed
48 lineaments on the seafloor that are readily observed in multibeam bathymetric data (Gold et al., 2017;
49 Fig. 1).



50
51 **Fig. 1. ASTER digital elevation and bathymetric multibeam data provided by TGS of the Biak Basin and**
52 **islands of Biak and Supiori displaying key structural and bathymetric features (MTDs - Mass transport**
53 **deposits).**

54 Several unusual geomorphologic collapse features are observed along the southern margin of the
55 offshore Biak Basin (Fig. 1). This study aims to test whether these features are fault-controlled or
56 diagenetic in origin by examining the bathymetric expression of structural features of the basin using
57 multibeam imagery and the burial history of analogous outcrop samples collected from formations that
58 extend offshore. This paper contributes to the understanding of geomorphologic and diagenetic
59 responses to regional tectonic events in a frontier basin of Eastern Indonesia through application of
60 laboratory techniques to identify the sedimentary processes that control geomorphologic features.

61

62 **2. Neogene geological history**

63 During the Early to Middle Miocene, carbonate platforms flourished across much of the Bird's
64 Head and are recorded in outcrop and the Salawati, Bintuni, and Biak Basins. These carbonates form
65 part of the 'New Guinea Limestone Group' which includes several contemporaneous carbonate
66 formations found across much of western New Guinea (Visser and Hermes 1962; Pieters et al. 1983;
67 Brash et al. 1991; Gold et al., 2017). From the Middle to Late Miocene, a reduction of carbonate
68 accumulation rates due to environmental deterioration which were outpaced by the rate of relative sea-
69 level rise led to the drowning of the New Guinea Limestone Group platform beneath deep-water strata
70 (Gold et al., 2017).

71 Rapid uplift of New Guinea, validated by fission track ages of metamorphic units, is recorded
72 from 10 Ma, and in many areas since 5 Ma (Hill and Gleadow, 1989). This culminated in the
73 formation of the regional 'intra-Pliocene unconformity', dated within the Salawati basin to have
74 occurred at approximately 4 Ma (Decker et al. 2009). This unconformity is related to rapid uplift of
75 the Misool-Onin-Kumawa ridge, an arcuate anticline sub-parallel to what is now the Seram Trough
76 (Pairault et al., 2003). The collision of the Banda Arc with the Australian margin in the Timor area
77 caused large scale surface deformation across the Bird's Head and Banda Arc from slab-mantle
78 decoupling (Spakman and Hall, 2010). The rapid isostatic uplift resulting from this decoupling caused
79 the formation of this unconformity and the rapid exhumation of the Neogene sediments.

80 The Biak Fault Zone is interpreted to be a young feature as it incises Pliocene strata (Gold et al.,
81 2017). Recent sedimentation within the Biak Basin is controlled by activity along the Biak Fault Zone
82 (Bertoni and Garcia 2012; Memmo et al. 2013).

83

84 **3. Investigation of offshore features**

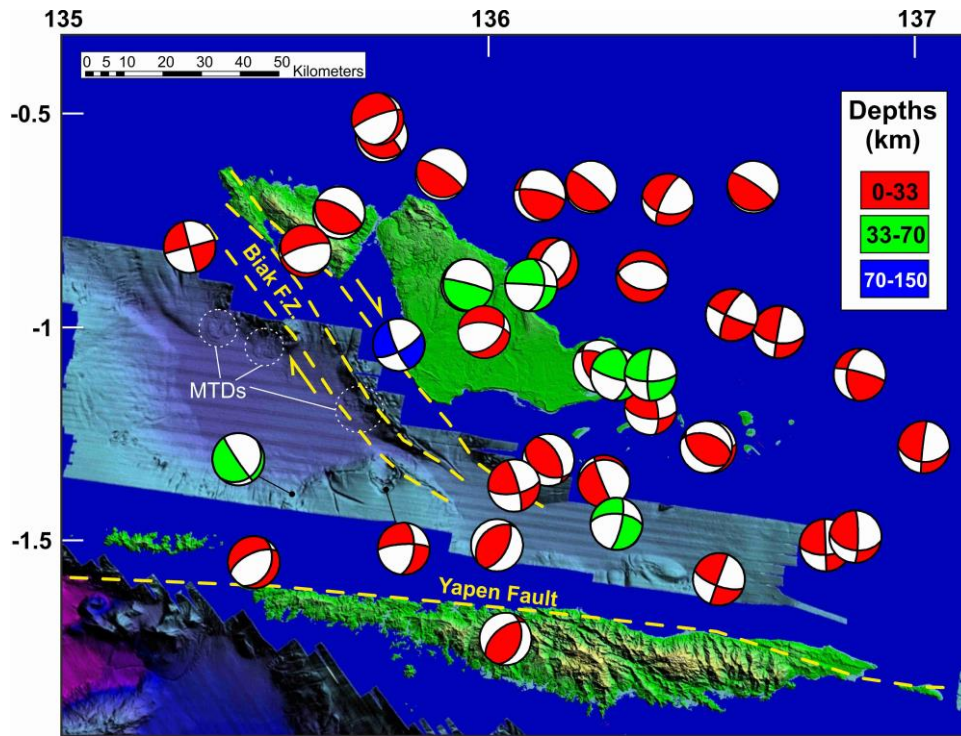
85 'Pock marks', headless canyons and semi-circular collapse features observed in bathymetric
86 multibeam data occur several kilometres offshore south-west of the island of Biak (Fig. 1). In
87 multibeam data, a narrow 'Y-shaped' headless canyon oriented NW-SE is approximately 10 km in
88 length and 700 m wide (Fig. 1). Approximately 20 km east of this structure, a semi-circular collapse
89 feature is approximately 7 km in diameter (Fig. 1). The potential for these structures to be fault-
90 controlled or diagenetic in origin was examined.

91

92 *3.1. Active faulting on the Biak margin*

93 The 'Y-shaped' canyon and semi-circular collapse structure are situated west of NW-SE striking
94 segments of the Biak Fault Zone which forms a transtensional flower structure to the east of the Biak
95 Basin (Fig. 1). The orientation of the 'Y-shaped canyon' and semi-circular collapse structures is also
96 NW-SE and are parallel to the strike of the Biak Fault Zone (Fig. 1). Recent earthquake CMT focal
97 mechanisms in the Biak and Supiori region plotted between 1st January 1976 and 1st January 2018
98 show that the Biak Fault Zone is currently seismically active (Fig. 2). Focal mechanisms indicate that
99 presently principal displacement along the Biak Fault Zone has a dextral strike-slip component along a
100 NW-SE striking plane parallel to the orientation of the faults identified in multibeam bathymetry (Fig.
101 2). Lobate mass transport deposits (MTDs) are common along strands of the Biak Fault Zone,
102 indicating the shedding of material during fault movement (Fig. 2), however they are absent from the
103 collapse structures on the southern margin of the Biak Basin. The 'Y-shaped' canyon displays no
104 evidence for seismicity within the last 40 years, nor is it associated with any MTDs (Fig. 2). The semi-
105 circular collapse structure is associated with an earthquake that occurred on 24th November 1990 at a

106 depth of 15 km, however this may be related to the slumping of overlying material into the collapse
107 feature.



108
109 **Fig.2. Recent earthquake CMT focal mechanisms in the Biak and Supiori region plotted from the**
110 **International Seismological Centre catalogue using MIRONE software in between 1st January 1976 to 1st**
111 **January 2018. Focal mechanisms are plotted over ASTER DEM and multibeam bathymetric imagery.**
112 **Mass transport deposits (MTDs) are common along strands of the Biak Fault Zone (Biak F.Z.) which**
113 **exhibit a predominantly dextral strike-slip component along computed fault planes that are parallel to**
114 **structures observed in multibeam bathymetry. MTDs are absent from the collapse structures on the**
115 **southern margin of the Biak Basin. The ‘Y-shaped’ canyon displays no evidence for seismicity within the**
116 **last 40 years, nor is it associated with any MTDs. The circular collapse structure is associated with an**
117 **earthquake that occurred on 24th November 1990 at a depth of 15 km displaying oblique slip with either a**
118 **dextral N-S component, possibly relating to the Biak F.Z., or a sinistral E-W component. However, this**
119 **earthquake may also have been related to the collapse of overlying material into an undercut cavity.**

120
121 The surface expression of the ‘Y-shaped’ canyon and semi-circular collapse feature is markedly
122 different to that of the Biak Fault Zone (Figs. 1 & 2). Segments of pure strike-slip often appear as
123 straight or wavy faults of modest topographic expression (Le Pichon et al., 2001). This is clearly

124 shown along the principal strands of the Biak Fault Zone which are laterally continuous, with evidence
125 for displacement and high relief fault scarps between minor faults parallel to the main strands of the
126 transtensional flower structure (Fig. 1). In contrast, the ‘Y-shaped’ canyon is observed in low relief
127 except for a deep narrow incision along its central course. Neither the ‘Y-shaped’ canyon nor the semi-
128 circular collapse feature display evidence for displacement or lateral continuity. It is, therefore,
129 interpreted that these structures are isolated and are not fault-controlled by activity of the Biak Fault
130 Zone.

131

132 3.2. *Submarine spring sapping*

133 The erosional undercutting of a slope results in mass wasting of overlying material (Orange and
134 Breen, 1992) and is known by a variety of terms including ‘seepage erosion’ (Hutchinson, 1968),
135 ‘artesian sapping’ (Milton, 1973) and ‘spring sapping’ (Johnson, 1939; , Small, 1965; Bates and
136 Jackson, 1980; Robb, 1990). In this article the term submarine spring sapping is favoured. There are
137 many examples of where spring sapping has resulted in the formation of submarine canyons
138 worldwide (e.g. Johnson, 1939, Robb, 1984; Paull and Neumann, 1987; Paull et al, 1990; Robb, 1990;
139 Orange and Breen, 1992; Orange et al., 1994; Dugan and Flemings, 2000; 2002; Green et al., 2007;
140 Flemings et al., 2008; Bratton, 2010).

141 Lateral migration of meteoric water within marine basins is well documented (Wu and Chafetz,
142 2002; Bratton, 2010). Bratton (2010) defined three spatial scales of submarine groundwater discharge:
143 1) nearshore – 0-10 m offshore, 2) embayment – 10 m – 10 km offshore, 3) shelf – width of the entire
144 continental shelf. Fresh water has been reported in a well 100 km off shore Florida in the Gulf of
145 Mexico, 10 km offshore of Saudi Arabia and offshore Bahrain in the Persian Gulf, and beneath the
146 continental shelves of the North Atlantic (Kohout, 1966; Fetter, 1980; Chafetz et al., 1988; Chafetz
147 and Rush, 1995; Edmonds, 2001; Wu and Chafetz, 2002; Person et al., 2003; Fleury et al., 2007).
148 Meteoric diagenesis of ancient carbonates through lateral flow of fresh water in palaeoquifers is also
149 well-documented (Grover and Read, 1983; Dorobek, 1987; Niemann and Read, 1987; Wu and
150 Chafetz, 2002; Moore and Wade, 2013).












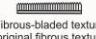









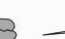

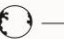




151 Submarine spring sapping results in headward erosion and slope undercutting that leads to
152 repeated slope failure and the formation of gullies and/or canyons (Orange and Breen, 1992). Orange
153 and Breen (1992) attribute the cause of spring sapping to be seepage induced slope failure controlled
154 by critical pore pressure gradients whereby flow through a porous medium exerts a force on grains
155 greater than the frictional or cohesive force holding the grains in place and material is transported
156 away leading to slumping of overlying material. It has been suggested that this process may be the
157 most significant mechanism for causing slope failure leading to the development of headless canyons
158 (Johnson, 1939; Sangrey, 1977).

159 Due to the isolated nature of the collapse features, and their tendency to form headless canyons,
160 the potential for these structures to be created through a process of submarine spring sapping was
161 examined. Carbonate units that are exposed on the islands of Biak and Supiori are interpreted to
162 extend into the offshore Biak Basin (e.g. Gold et al., 2014). Therefore, samples were collected from
163 Biak and Supiori to determine whether evidence for meteoric diagenesis is observed onshore in units
164 interpreted to be present in the subsurface of the Biak Basin.

165

166 **4. Material and methods of onshore analogue analyses**

167 Fieldwork was conducted in 2011 and 2013 on the islands of Biak and Supiori. Carbonates were
168 described in the field and sampled for analysis at Royal Holloway, University of London. In total 47
169 samples were selected for petrographic analyses using thin section petrography to determine their post-
170 depositional burial history. Cement types observed during petrographic analysis were divided into
171 those that form in meteoric waters, the marine realm, and shallow and deep burial environments based
172 on features described by Tucker and Wright (1990) and Scholle and Ulmer-Scholle (2003), and
173 depicted in Figure 3.

Stage	Fluids	Environment	Features	Mineralogy	
Early Diagenesis	Freshwater	Meteoric Vadose	  Microstalactitic/Pendant Structure - Formed from hanging water droplets Rounded ϕ	Early meteoric exposure and flushing of meteoric pore fluids results in leaching of aragonitic grains leading to secondary ϕ (possibly leaving only micrite envelopes) Aggrading neomorphic replacement of micrite mud to micro-/pseudospars	Mineralogy of features (e.g. fibrous aragonite or microcrystalline HMC) will provide evidence of depositional environment, aforementioned marine minerals will imply a coastal spray zone, for example Non-ferroan LMC spar cements
		Meteoric Phreatic	   		
	Marine	      	Non-ferroan aragonite, microcrystalline HMC. Marine cements form rapidly and are therefore inclusion rich leading to brown, cloudy colours in PPL		
Late Diagenesis	Pore Fluids	Shallow Burial	      	Ferroan calcite in reducing conditions. Thin dolomite rinds on HMC marine cements	
		Deep Burial	       	Ferroan calcite spar and dolomite in reducing conditions. Depleted in Mn, enriched in Fe gives a dull cathodoluminescence. Inclusions are often absent	

174

175

Fig. 3. Features of carbonate cement fabrics and textures observed within different diagenetic

176

environments: ϕ - Porosity; LMC - Low Magnesian Calcite; HMC - High Magnesian Calcite; PPL - Plane

177

Polarised Light (after Tucker and Wright, 1990; Scholle and Ulmer-Scholle, 2003).

178

179

Nine samples (Biak 1-5, Supiori 1-4) deemed representative of the varying diagenetic cement

180

types identified through thin section petrography were later selected for bulk-rock stable isotope ($\delta^{18}\text{O}$

181

and $\delta^{13}\text{C}$) analyses to determine the presence of meteoric cements. Samples were milled to extract

182

powdered calcite specifically from areas in which cements were abundant, avoiding bioclastic grains

183

to ensure bulk isotope values indicative of diagenetic cement. Carbon dioxide was extracted from

184

samples by reacting the milled powder with phosphoric acid using the procedure described by McCrea

185

(1950). Three standards were used to fix the calibration curve, NBS19, LSVEC, and RHBNC.

186

RHBNC is the Royal Holloway standard taken from Iceland spar which forms at low temperatures.

187

One standard was used for NBS19 and LSVEC, and three samples of RHBNC were used as a control

188

to monitor the run. Analytical precision, based on the RHBNC standard, was less than 0.05‰ for both

189

oxygen and carbon ratios (Table 1). Consistency of results was achieved by comparing laboratory

190

standards against NBS19 using the calibration curve. The stable isotope data are recorded in relation to

191

the heavier isotope ($\delta^{18}\text{O}$ and $\delta^{13}\text{C}$), and Pee Dee Belemnite (VPDB) standard.

192

193 **5. Petrographic analysis**

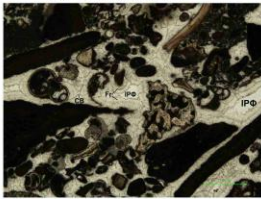
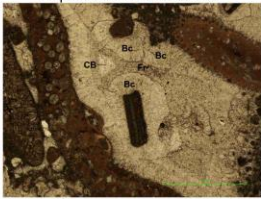




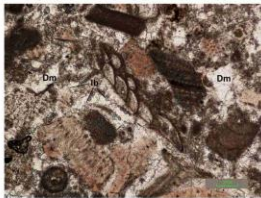


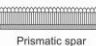

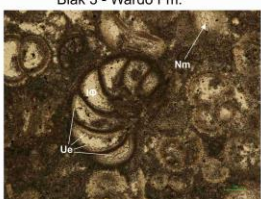


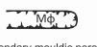

194 The diagenetic features of the samples including porosity forming episodes, cross cutting
195 relationships, and overgrowth of cements was examined (Fig. 4). Different carbonate cement textures
196 and fabrics form within different diagenetic environments relating to the chemistry of the waters they
197 are bathed in, saturation with respect to carbonate, and levels of oxygen upon burial (Fig. 2).

198

199 *5.1. Description*

200 Samples Biak 1 of the Pleistocene age Mokmer Formation and Supiori 1 of the Early Miocene
201 age Wainukendi Formation are classified as grainstones which contain inclusion-rich fibrous fringes
202 and botryoidal cements, with intervening primary interparticle porosity (Fig. 4). The remainder of the
203 samples which are Pliocene age or older (Biak 2-5, Supiori 2-4) contain abundant isopachous or
204 uneven bladed calcite cements fringing grains, pore-filling inclusion-free equant calcite cements and a
205 packstone fabric undergoing aggrading neomorphism of originally aragonitic micrite to calcite micro-
206 or pseudospar (Fig. 4). This fabric is later cross cut by the development of secondary mouldic porosity
207 (Fig. 4).

208

Diagenetic Zone	Petrography		Features
MARINE	Biak 1 - Mokmer Fm. 	Supiori 1 - Wainukendi Fm. 	 HMC micrite envelopes (ME)  Primary interparticle porosity (IPΦ)  Fringe (Fr), often cloudy, with radial-fibrous texture, isopachous fabric often meet to form compromise boundaries (CB)  Botryoidal cements (Bc)
	Supiori 2 - Wainukendi Fm. 	Biak 5 - Wafordori Fm. 	 Isolated bladed calcite (Ib)  Prismatic spar overgrows marine cements (Og)  Blocky-equant texture, drusy fabric mosaics (Dm)
METEORIC PHREATIC	Biak 3 - Wardo Fm. 	Biak 4 - Wafordori Fm. 	 Aggrading neomorphism (Nm)  Secondary mouldic porosity of leached (preferentially aragonitic) grains often surrounded by micrite envelopes (ME)  Uneven, equant-bladed texture (Ue)

209

210 **Fig. 4. Thin section photographs in plane polarised light of cement textures and fabrics observed during**
211 **petrographic analysis of samples. Different cement textures and fabrics are observed to be characteristic**
212 **of the marine, shallow burial and meteoric phreatic diagenetic realms.**

213

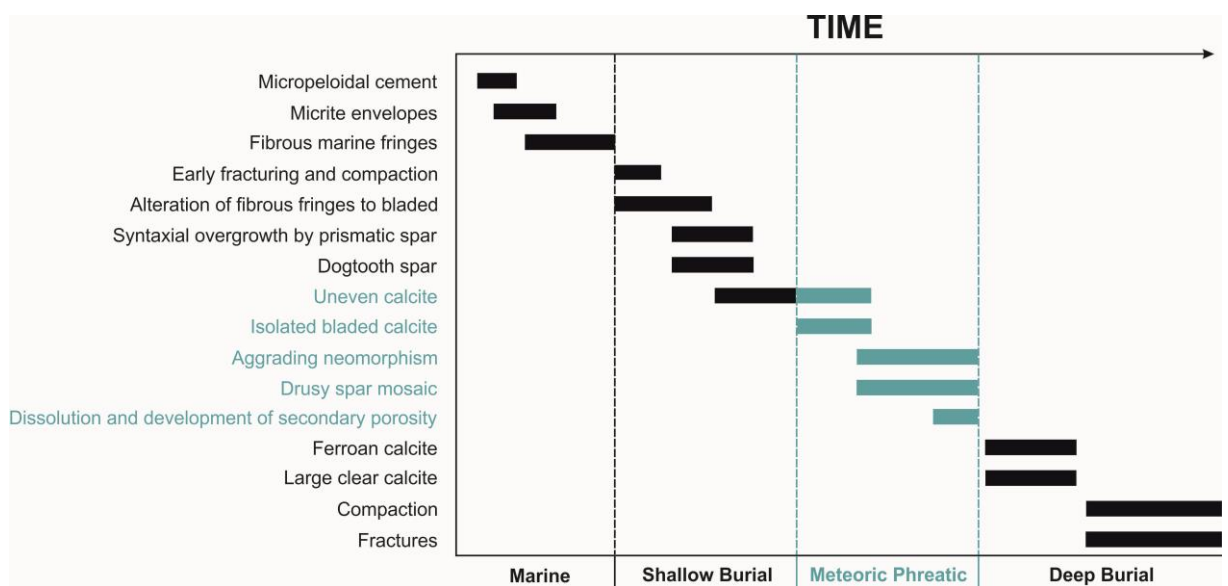
214 *5.2. Interpretation*

215 Samples from the relatively young Pleistocene age sediments of the Mokmer Formation are
216 interpreted to have been deposited in a reefal environment on the reef crest and reef front. These
217 environments are home to photosynthetic organisms and high hydrodynamic energies that act to
218 remove CO₂ away from the site of deposition. This increases alkalinity and encourages precipitation of
219 early marine cements such as fibrous fringes that often do not fully occlude interparticle pore space
220 (Figs. 3 & 4).

221 Sediments influenced by meteoric phreatic diagenesis are characterized by pervasive
222 calcitization of aragonite, extensive dissolution with well-developed mouldic porosity, and the
223 occurrence of isopachous bladed and pore-filling equant calcite cements (Quinn, 1991; Figs. 3 & 4).
224 Meteoric diagenesis is often responsible for aggressive dissolution and porosity enhancement due to

225 undersaturation of meteoric waters with respect to calcite and the development of secondary mouldic
 226 porosity (Tucker and Wright, 1990). These characteristics are observed in samples from Pliocene and
 227 older sediments, with the exception of sample Supiori 1 of the Wainukendi Formation. It is therefore
 228 interpreted that onshore samples from Biak and Supiori were subject to pervasive overprinting by
 229 meteoric cements which is likely to extend into the offshore. This supports Hendarjo and
 230 Netherwood's (1986) observations from the nearby Salawati Basin where most offshore samples were
 231 subject to meteoric phreatic diagenesis after burial.

232 Through petrographic analyses a paragenetic sequence of cement phases precipitated with
 233 increasing time and burial was determined based on cross-cutting and over-printing relationships (Fig.
 234 5). Over printing relationships suggest that they underwent diagenesis in a meteoric phreatic
 235 environment late on during their paragenetic history (Fig. 5).



236
 237 **Fig. 5. Paragenetic scheme of cement phases forming with increasing time and burial. Evidence for**
 238 **diagenesis in the marine, shallow burial, meteoric phreatic and deep burial diagenetic realms is**
 239 **interpreted. Based on overprinting relationships, the meteoric phreatic diagenetic realm is encountered**
 240 **late on in the paragenetic sequence.**

241

242 **6. Results of stable isotope analysis**

243 The results of the bulk-rock stable isotope analyses are given in Table 1. The results show that
 244 calcite comprised >94% of the powdered carbonate material in all but one sample. Sample Biak 3 of
 245 the Korem Formation contained only ca. 70% calcite. The $\delta^{18}\text{O}$ values of the calcite cements range
 246 from -5.36 to -1.48‰_{VPDB} (Table 1) and the $\delta^{13}\text{C}$ values range from -7.61 to +2.74‰_{VPDB} (Table 1).
 247 Carbon-oxygen cross plots of the analysed samples are shown in Figure 6.

Samples	Formation	Age	$\delta^{13}\text{C}(\text{‰})$	$\delta^{18}\text{O}(\text{‰})$	Est % carb.	$\delta^{18}\text{O}$ sea water	Temp (°C)	Depth (m)
Standards								
RHBNC			3.31	-10.37	95.49			
RHBNC			3.23	-10.35	102.36			
RHBNC			3.22	-10.42	96.00			
Average			3.25	-10.38	97.95			
External Precision			0.04	0.03				
NBS-19			1.94	-2.20	100.00			
Known			1.95	-2.20				
LSVEC			-46.50	-26.70	112.37			
Known			-46.50	-26.70				
Outcrop								
Biak 1	Mokmer	Pleistocene	2.66	-1.48	94.34	-1.20	17.2	572.3
Biak 2	Wardo	Pliocene	-7.21	-5.03	97.52	-1.20	33.8	1126.0
Biak 3	Wardo	Pliocene	-6.95	-3.79	71.92	-1.20	27.6	920.5
Biak 4	Wafordori	Middle - Early Miocene	-7.61	-4.81	98.23	-1.20	32.6	1087.7
Biak 5	Wafordori	Middle - Early Miocene	-2.44	-5.36	98.96	-1.20	35.5	1182.5
Supiori 1	Wainukendi	Early Miocene	2.74	-1.71	97.73	-1.20	18.1	604.8
Supiori 2	Wainukendi	Early Miocene	0.34	-2.52	95.91	-1.20	21.7	723.5
Supiori 3	Wainukendi	Early Miocene	0.84	-3.11	96.77	-1.20	24.4	813.4
Supiori 4	Wainukendi	Early Miocene	0.61	-4.56	95.64	-1.20	31.4	1046.8

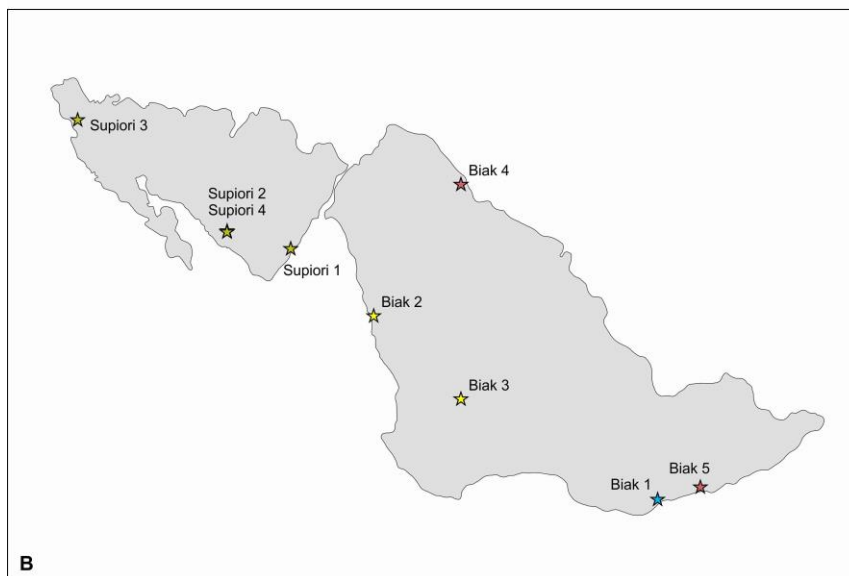
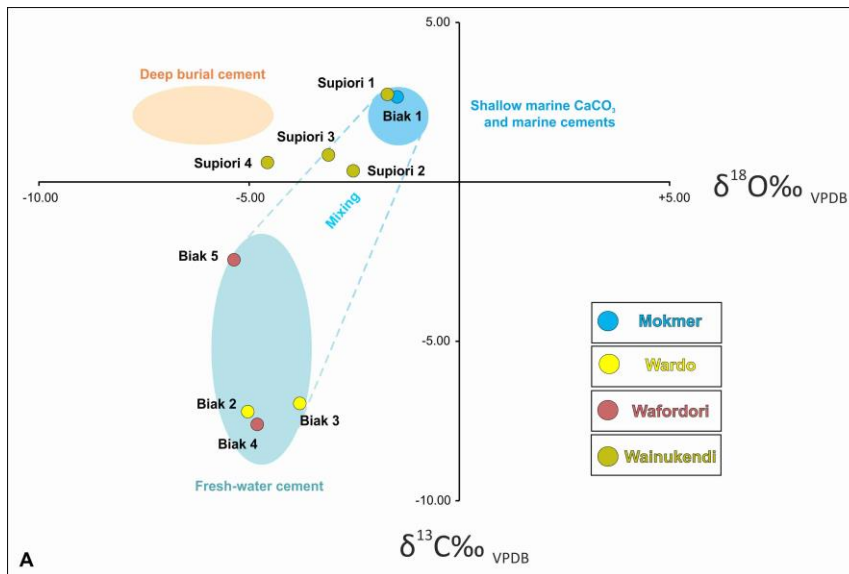
248

249 **Table 1. Oxygen and carbon isotope data including standards and precision information. The stable**
 250 **isotope data are recorded in relation to the heavier isotope ($\delta^{18}\text{O}$ and $\delta^{13}\text{C}$), and Peedee Belemnite**
 251 **(VPDB) standard. Isotopic composition of sea water taken from Shackleton and Kennett (1975).**

252 **Temperature calculated using method described by Anderson and Arthur (1983). Calculated burial depth**
253 **using a geothermal gradient of 3°C/100m.**

254

255 The results of the stable isotope analysis indicate that the majority of the cements show a trend
256 from precipitation in normal shallow marine waters to precipitation in the meteoric phreatic diagenetic
257 realm, supporting observations made through petrographic analysis (Fig. 6). Meteoric cements have
258 negative $\delta^{18}\text{O}$ values as fresh water is more enriched with the lighter ^{16}O isotope. However, during late
259 diagenesis pore fluids also often exhibit negative $\delta^{18}\text{O}$ values, and less negative $\delta^{13}\text{C}$, (Fig. 6) due to
260 higher temperatures of precipitation on burial and fractionation (Dickson and Coleman, 1980; Tucker
261 and Wright, 1990).



262
 263 **Fig. 6. A) Carbon-oxygen cross plots for Neogene carbonate samples analysed for stable isotope**
 264 **geochemistry. Samples Biak 1 and Supiori 1 which display obvious marine cements lay within the carbon**
 265 **and oxygen isotopic values expected for the precipitation of marine cements. There is a trend towards**
 266 **freshwater cements occurring during burial, supporting the interpretation of a submarine freshwater**
 267 **aquifer beneath the burial diagenetic environment. B) Location map of samples collected from the islands**
 268 **of Biak and Supiori**

269
 270 Samples Biak 1 and Supiori 1 of the Mokmer and Wainukendi Formations, respectively, plot
 271 close together in the low positive end of $\delta^{18}\text{O}$ and $\delta^{13}\text{C}$ values (Fig. 5). Both these samples exhibit very
 272 obvious early marine diagenetic features such as inclusion-rich fibrous fringes and botryoidal cements

273 (Fig. 4), and plot with carbon and oxygen isotope values expected for normal marine carbonate
274 cements (Fig. 6). Samples from the Wardo (Biak 2-3) and Wafordori (Biak 4-5) Formations exhibit
275 highly negative $\delta^{18}\text{O}$ values between -3.79 and -5.36‰ VPDB , typical of values expected of meteoric
276 phreatic cements (Fig. 6). The oldest Early Miocene samples from the Wainukendi Formation (Supiori
277 2-3) fall within the mixing zone between normal marine and meteoric phreatic cements (Fig. 5).
278 However, sample Supiori 4 of the Wainukendi Formation exhibits $\delta^{18}\text{O}$ and $\delta^{13}\text{C}$ values approaching
279 those expected for deep burial cements (Fig. 5).

280 The results of the bulk-rock stable isotope analyses allowed palaeothermometry calculations to
281 determine temperatures at which the cements precipitated. A geothermal gradient of $3^\circ\text{C}/100\text{m}$ was
282 calculated from bottom-hole temperatures in the similar Salawati (Redmond and Koesoemadinata,
283 1976), Bintuni (Chevallier and Bordenave, 1986), and North Irian (McAadoo and Haebig, 1999)
284 regional basins was used to convert temperature to depth.

285 The method for calculating palaeodepths and precipitation temperatures was taken from work
286 on the cement stratigraphy of Miocene carbonates from Sabah, Malaysia (Ali, 1995). It was assumed
287 that the parameters of Ali's (1995) method would closely match that of the Biak Basin since samples
288 used in both experiments were of similar age, latitude, geothermal and hydrothermal gradients, and
289 were likely to have similar starting sea-water temperatures and isotopic values.

290 To equate the calculated $\delta^{18}\text{O}_{\text{VPDB}}$ values obtained by mass spectroscopy to burial depth, it is
291 necessary to know the isotopic composition of the ambient pore fluids, the geothermal gradient for the
292 time of each cement stage, and the degree of openness of the system (Ali, 1995). As the isotopic
293 composition of the pore fluids is unknown, it is impossible to relate the $\delta^{18}\text{O}_{\text{VPDB}}$ values precisely to a
294 burial depth. However, an estimate of palaeo-precipitation temperature can be given using Equation 1.
295 This equation follows a standard palaeotemperature calculation given by Epstein et al. (1953), later
296 refined by Irwin et al. (1977) and Anderson and Arthur (1983), and used by Ali (1995) on Miocene
297 carbonates from Sabah.

298

299
$$T = 16.0 - 4.14 (\delta_c - \delta_w) + 0.13 (\delta_c - \delta_w)^2 \quad [\text{Eq.1}]$$

300 Where:

301 T = precipitation temperature ($^{\circ}\text{C}$)

302 δ_c = oxygen isotopic composition of CO_2 produced from calcite at 25°C

303 δ_w = oxygen isotopic composition of CO_2 in equilibrium with formation water, given as -1.2‰ for
304 seawater composition prior to the establishment of polar ice caps (Shackleton and Kennett, 1975; Ali,
305 1995).

$$306 \quad \quad \quad D = T/Gg \quad \quad \quad [\text{Eq.2}]$$

307 Where:

308 D = depth (m)

309 T = precipitation temperature ($^{\circ}\text{C}$) calculated using Equation 1

310 Gg = geothermal gradient, here given as $3^{\circ}\text{C}/100\text{m}$ (0.03)

311

312 Using the $3^{\circ}\text{C}/100\text{m}$ geothermal gradient, maximum burial depth can be calculated using
313 Equation 2. From the recorded values of $\delta^{18}\text{O}$, it is calculated that meteoric cements from sample Biak
314 5 of the Wafordori Formation attained the greatest burial depth and temperature values of ca. 1.2 km
315 and ca. 35.5°C , respectively (Table 1).

316

317 **7. Discussion**

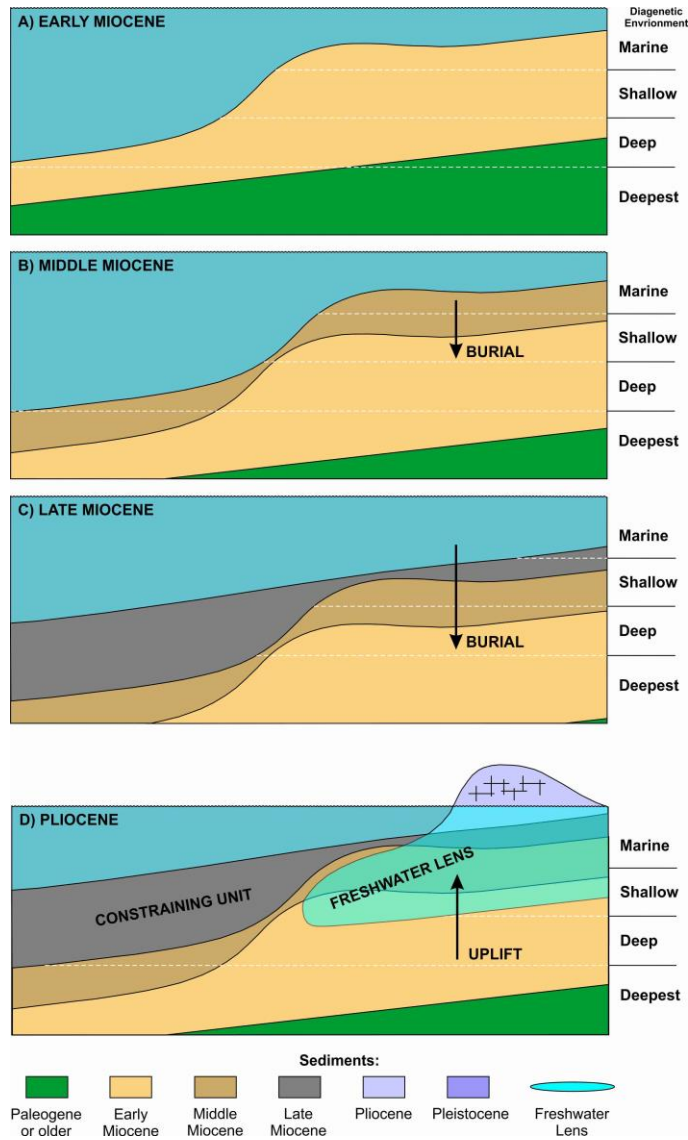
318 *7.1. Synthesis of petrographic and stable isotopic data*

319 Carbonate cements that have undergone meteoric phreatic diagenesis specifically related to
320 subaerial exposure are reported to display variable $\delta^{13}\text{C}$ values with relatively constant $\delta^{18}\text{O}$ values
321 (Allan and Matthews, 1982). However, relatively constant $\delta^{13}\text{C}$ and variable $\delta^{18}\text{O}$ values are an
322 indicator of meteoric diagenesis at relatively low water-rock ratios (Wu and Chafetz, 2002). Samples
323 from Biak and Supiori display increasingly negative $\delta^{18}\text{O}$ and $\delta^{13}\text{C}$ values which indicate considerable
324 water-rock interactions suggesting meteoric waters had a progressively greater influence on the
325 isotopic composition of samples during burial (e.g. Wu and Chafetz, 2002).

326 Observations of overprinting of cements indicate that meteoric diagenesis occurred late on in the
327 paragenesis of the carbonate samples (Fig. 5). This is supported by the temperatures calculated for the
328 precipitation of meteoric cements during stable isotope analysis which suggest they were precipitated
329 at depths ca. 1 km (Table 1). During the Early to Middle Miocene, carbonates originally formed in the
330 marine diagenetic environment were progressively buried, passing through underlying diagenetic
331 environments precipitating deeper burial cements (Fig. 5).

332 Samples dated from the Early Miocene through to the Pliocene are interpreted to have attained
333 burial depths of approximately 1.2 km (Table 1). This suggests relatively rapid uplift of Neogene strata
334 since the Pliocene. There may have been gradual burial of carbonate strata in the Bird's Head region
335 up to the Pliocene until the formation of the regional 'Intra-Pliocene' unconformity at 4 Ma (Decker et
336 al., 2009) which is responsible for the rapid exhumation of Neogene sediments.

337 Meteoric phreatic diagenesis within carbonate rocks is usually attributed to periods of low
338 relative sea-level, especially within shallow water facies rocks (Meyers and Lohmann, 1985; Quinn,
339 1991; Frank and Lohmann, 1995; Melim, 1996; Moore and Wade, 2013). Karstic joints that are
340 developed in subaerially exposed carbonates of the hinterland act as a conduit for freshwater aquifers
341 to extend offshore. In the Biak and Supiori region, relative sea-level lowstand is attributed to the
342 tectonic uplift, exhumation subaerial exposure and karstification of the youngest Neogene sediments
343 during the formation of the 'Intra-Pliocene' unconformity (Fig. 7). Karstic joints acted as conduits for
344 freshwater to develop a subterranean lens bathing older strata in meteoric waters. It is interpreted that
345 this freshwater lens is the cause of meteoric phreatic diagenesis within samples analysed by this study.
346 The process of exhumation uplifted strata previously buried within deep diagenetic environments up
347 into the region influenced by the freshwater lens, causing overprinting of meteoric cements on
348 interpreted burial cements (Fig. 7).



349
350
351
352
353
354
355
356
357
358
359
360

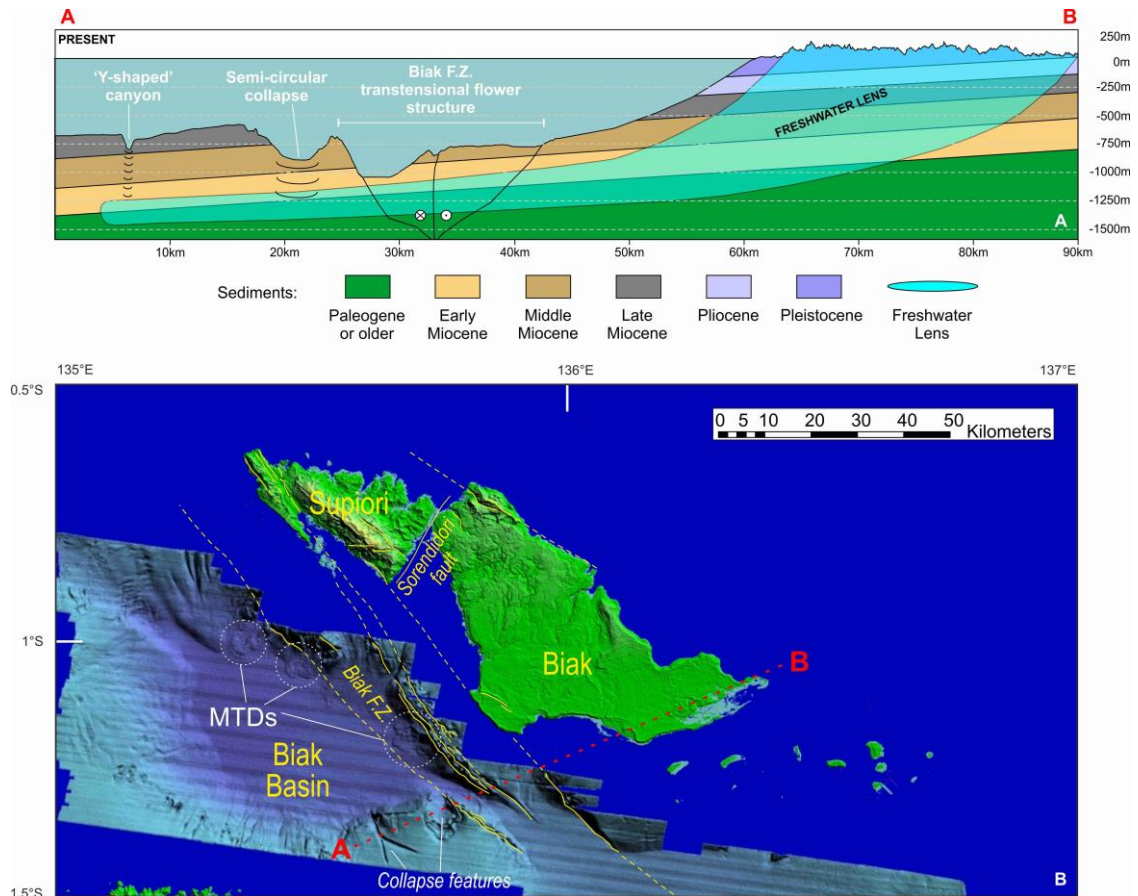
Fig. 7. Schematic model showing development of the freshwater lens during the Neogene. A) During the Early Miocene, carbonate platforms grow within marine diagenetic realms, burying older to deeper burial diagenetic environments, B) As relative sea-level rises, Middle Miocene carbonate strata backstep across former Early Miocene platform, burying it within the shallow burial diagenetic realm, C) As relative sea-level continues to rise, the Early Miocene platform is progressively buried to deeper diagenetic environments, D) Uplift forming the intra-Pliocene unconformity exposes Pliocene sediments. Karstification forms conduits for freshwater lens to develop and penetrate older strata. Strata previously buried within deep diagenetic environments are uplifted into meteoric realm causing overprinting of meteoric diagenesis over burial cements. The oldest sediments are not uplifted far enough to reach fresh water lens and retain deepest burial diagenetic signature.

361 Some of the oldest Early Miocene samples from the Wainukendi Formation exhibit carbon and
362 oxygen isotopic values close to those expected for deep burial cements (Fig. 6). It is interpreted that
363 these samples have not been uplifted through the freshwater lens, and are exposed updip of the lens on
364 the island of Biak. Inversely, the youngest Pleistocene sediments have not been buried to such an
365 extent to have reached the freshwater lens, and remain unaffected by meteoric diagenesis (Fig. 8).

366

367 7.2. *Effect of meteoric diagenesis in the Biak Basin*

368 ‘Pock mark’ and collapse features, such as those observed west of Biak and Supiori (Fig. 1), are
369 often associated with gas seepage (e.g. Hovland and Judd, 1998; Yun et al., 1999). However, here they
370 are interpreted to be caused by submarine ‘spring sapping’. The process of submarine spring sapping
371 is interpreted to be driven by the freshwater lens responsible for the meteoric phreatic overprinting of
372 samples collected onshore Biak and Supiori extending a considerable distance offshore (Fig. 8). The
373 Biak and Supiori aquifer extending offshore into the Biak Basin represents the shelf scale of Bratton
374 (2010). At the shelf scale the freshwater aquifer extends as far as the shallowest overlying confining
375 unit, typically comprising fine-grained sediments (Bratton, 2010). The confining unit in Biak and
376 Supiori are interpreted to be Late Miocene to Pliocene deep water sediments (e.g. Gold et al., 2017).
377 The thickness of the meteoric lens at the shelf scale is typically several hundred metres and has a width
378 of approximately 80km (Bratton, 2010). In the offshore Biak Basin the width of the lens extends
379 approximately 55 km offshore and is interpreted to be approximately 250 m thick (Fig. 8). The
380 interpreted ca. 1 km depth of the Biak freshwater lens is comparable to that of the Floridian Aquifer
381 and extends almost as far offshore (Fig. 8).



382
 383 **Fig. 8. A) Present day topographic and bathymetric profile along transect A-B across southern Biak and**
 384 **into the offshore Biak Basin. The freshwater lens extends southwest from the island beneath the Biak**
 385 **basin, comparable to the Floridian Aquifer. B) Transect A-B displayed in map view across the southern**
 386 **margin of the Biak Basin**

387

388 It is unknown whether the 'Y-shaped' canyon or semi-circular collapse feature observed in
 389 multibeam bathymetry (Fig. 8) formed during subaerial exposure or subaqueously. However, it is
 390 likely that both are relatively recent structures, no older than the Pliocene. The lateral, rather than
 391 vertical, displacement of carbonate units by the Biak Fault Zone permitted the freshwater lens to
 392 extend beyond the transensional flower structure via well-developed karstic joints acting as conduits
 393 to the southern margin of the Biak Basin.

394

395 **8. Conclusions**

396 Petrographic and stable isotope analysis of Neogene carbonates from the Bird's Head region of
397 New Guinea enables the reconstruction of their subsequent burial history and potential as hydrocarbon
398 reservoirs. The following conclusions can be drawn from these reconstructions.

399 Calculation of burial temperatures and depths reached by samples suggest that they attained a
400 maximum temperature of ca. 35.5°C and depth of ca. 1.2 km up until the Pliocene. Sediments were
401 rapidly exhumed during the creation of the 'intra-Pliocene unconformity' formed when rapid isostatic
402 uplift as slab-mantle decoupling close to Timor affected the wider Banda Arc and Bird's Head region.
403 This uplift resulted in a period of low relative sea-level in the Biak and Supiori region with the
404 development of a freshwater aquifer formed as a response. Most samples show evidence of meteoric
405 phreatic diagenesis through petrographic recognition of meteoric cements and presence of light oxygen
406 isotopes. Precipitation of these cements is interpreted to have occurred late on in the paragenetic
407 history of the samples as they passed through a freshwater lens during uplift. Subsequent 'spring
408 sapping' by this freshwater lens is responsible for various collapse structures observed in multibeam
409 bathymetry of the Biak Basin.

410

411 **Acknowledgments**

412 I would like to thank TGS for providing multibeam bathymetric data, Ramadhan Adhitama and Ferry
413 Yulien of Institut Teknologi Bandung for assistance during field work and collection of the samples,
414 the Southeast Asia Research Group consortia and staff members at Royal Holloway, University of
415 London for enabling this study to take place, Dr. Dave Lowry and Dr. Nathalaie Grassineau for help in
416 stable isotope analysis, and Dr. Jim Hendry for continued support and assistance in the production of
417 the isotope cross plot. Finally, I would like to thank Robert Hall for continued mentoring, guidance,
418 helpful discussion and facilitating the progression of our understanding of a geologically complex and
419 exciting region of the world through his work with the Southeast Asia Research Group.

420

421 **Funding**

422 This research was funded by industrial companies as part of a consortium supporting the Southeast

423 Asia Research Group at Royal Holloway, University of London.

424

425 Declarations of interest: None

426 **References**

427 Ali, M. Y., 1995. Carbonate cement stratigraphy and timing of diagenesis in a Miocene mixed
428 carbonate-clastic sequence, offshore Sabah, Malaysia: constraints from cathodoluminescence,
429 geochemistry, and isotope studies. *Sedimentary Geology* 99 (3), 191-214.

430

431 Allan, J.R., Matthews, R.K., 1982. Isotope signatures associated with early meteoric diagenesis.
432 *Sedimentology* 29(6), 797-817.

433

434 Bertoni, C., Garcia, J.A., 2012. Interplay between Submarine Depositional Processes and Recent
435 Tectonics in the Biak Basin, Western Papua, Eastern Indonesia. *Berita Sedimentologi* 23, 42-45.

436

437 Bratton, J.F., 2010. The three scales of submarine groundwater flow and discharge across passive
438 continental margins. *The Journal of Geology* 118(5), 565-575.

439

440 Chafetz, H. S., McIntosh, A. G., Rush, P.F., 1988. Freshwater diagenesis in the marine realm of recent
441 Arabian Gulf carbonates. *Journal of Sedimentary Petrology* 58 (3), 433-440.

442

443 Chafetz, H.S., Rush, P.F., 1995. Two-phase diagenesis of Quaternary carbonates, Arabian Gulf:
444 Insights from $\delta^{13}\text{C}$ and $\delta^{18}\text{O}$ data. *Journal of Sedimentary Research* A65, 294–305.

445

446 Chevallier, B., Bordenave, M. L., 1986. Contribution of geochemistry to the exploration in the Bintuni
447 Basin, Irian Jaya. *Proceedings Indonesian Petroleum Association, 15th Annual Convention and*
448 *Exhibition, Jakarta, 439-460.*

449

450 Decker, J., Bergman, S.C., Teas, P.A., Baillie, P., Orange, D.L., 2009. Constraints on the tectonic
451 evolution of the Bird's Head, West Papua, Indonesia. *Proceedings Indonesian Petroleum Association,*
452 *33rd Annual Convention and Exhibition, Jakarta, 491-514, IPA-G-139.*

453

454 Dickson, J.A.D., Coleman, M.L., 1980. Changes in carbon and oxygen isotope composition during
455 limestone diagenesis. *Sedimentology* 27(1), 107-118.

456

457 Dorobek, S.L., 1987. Petrography, geochemistry, and origin of burial diagenetic facies, Siluro-
458 Devonian Helderberg Group (carbonate rocks), Central Appalachians. *AAPG Bulletin* 71, 492–514.

459

460 Dugan, B., Flemings, P.B., 2002. Fluid flow and stability of the U.S. continental slope offshore New
461 Jersey from the Pleistocene to the present. *Geofluids* 2,137–146.

462

463 Dugan, B., Flemings, P.B., 2000. Overpressure and fluid flow in the New Jersey Continental Slope:
464 implications for slope failure and cold seeps. *Science* 289, 288–291.

465

466 Epstein, S., Buchsbaum, R., Lowenstam, H.A., Urey, H.C., 1953. Revised carbonate-water isotopic
467 temperature scale. *Geological Society of America Bulletin* 64 (11), 1315-1326.

468

469 Fetter, C.W., 1980. *Applied hydrogeology*. Charles E. Merrill Publishing, Toronto.

470

471 Flemings, P.B., Long, H., Dugan, B., Germaine, J., John, C., Behrmann, J.H., Sawyer, D., Expedition
472 IODP, 2008. Pore fluid overpressure measured with penetrometers on the continental slope, Gulf of
473 Mexico. *Earth and Planetary Science Letters* 269, 309–324.

474

475 Fleury, P., Bakalowicz, M., de Marsily, G., 2007. Submarine springs and coastal karst aquifers: a
476 review. *Journal of Hydrology* 339 (1), 79-92.

477

478 Frank, T.D., Lohmann, K.C., 1995. Early cementation during marine-meteoric fluid mixing:
479 Mississippian Lake Valley Formation, New Mexico. *Journal of Sedimentary Research* A65, 263–273.

480

481 Gold, D.P., Hall, R., Burgess, P., BouDagher-Fadel, M.K., 2014. The Biak Basin and its setting in the
482 Bird's Head region of West Papua. Proceedings, Indonesian Petroleum Association Thirty-Eighth
483 Annual Convention and Exhibition, IPA14-G-298:448-460

484

485 Gold, D.P., Burgess, P.M., BouDagherFadel, M.K., 2017. Carbonate drowning successions of the
486 Bird's Head. *Facies* 63(4), 25.

487

488 Green, A.N., Goff, J.A., Uken, R. 2007. Geomorphological evidence for upslope canyon-forming
489 processes on the northern KwaZulu-Natal shelf, SW Indian Ocean, South Africa. *Geo-Marine Letters*
490 27, 399–409.

491

492 Grover, G., Jr, Read, J.F., 1983. Paleoaquifer and deep burial related cements defined by regional
493 cathodoluminescent patterns, Middle Ordovician carbonates, Virginia. *AAPG Bulletin* 67, 1275–1303.

494

495 Hendarjo, K.S., Netherwood, R.E., 1986. Palaeoenvironmental and diagenetic history of Kais
496 Formation, KBSA, Irian Jaya. Proceedings Indonesian Petroleum Association, 15th Annual Convention
497 and Exhibition, Jakarta, 423-438.

498

499 Hill, K.C., Gleadow, A.J.W., 1989. Uplift and thermal history of the Papuan Fold Belt, Papua New
500 Guinea: Apatite fission track analysis. *Australian Journal of Earth Sciences* 36(4), 515-539.

501

502 Hovland, M., Judd, A.G., 1988. Seabed pockmarks and seepages. Impact on geology, biology and the
503 marine environment. Graham and Trotman Ltd., London.

504

505 Hutchinson, J. N., 1968. Mass movement. In: Fairbridge, R.W. (Ed.), *Encyclopedia of*
506 *Geomorphology*. von Nostrand Reinhold, New York, 1295 pp.

507

508 Irwin, H., Curtis, C., Coleman, M., 1977. Isotopic evidence for source and diagenetic burial of
509 organic-rich sediments. *Nature* 269, 209-213.

510

511 Johnson, D., 1939. *The Origin of Submarine Canyons: A Critical Review of Hypotheses*. Columbia
512 University Press, New York.

513

514 Kohout, F. A., 1966. Submarine springs. In: Fairbridge, R. W. (Ed.) *Encyclopedia of the Earth
515 Sciences, Vol. 1, Oceanography*, von Nostrand Reinhold, New York, 878-883.

516

517 Le Pichon, X., Şengör, A.M.C., Demirbağ, E., Rangin, C., Imren, C., Armijo, R., Görür, N., Çağatay,
518 N., De Lepinay, B.M., Meyer, B., Saatçılar, R., 2001. The active main Marmara fault. *Earth and
519 Planetary Science Letters*, 192(4), 595-616.

520

521 McAdoo, R.I., Haebig, J.C., 1999. Tectonic elements of the north Irian Basin. *Proceedings Indonesian
522 Petroleum Association, 27th Annual Convention and Exhibition, Jakarta, IPA99-G-150, 1-17.*

523

524 McCrea, J.M., 1950. On the isotopic chemistry of carbonates and a paleotemperature scale. *Journal of
525 Chemical Physics* 18 (6), 849-857.

526

527 Melim, L.A., 1996. Limitations on lowstand meteoric diagenesis in the Pliocene-Pleistocene of Florida
528 and Great Bahama Bank: Implications for eustatic sea-level models. *Geology* 24(10), 893-896.

529

530 Memmo, V., Bertoni, C., Masini, M., Alvarez, J., Imran, Z., Echanove, A., Orange, D., 2013.
531 Deposition and deformation in the recent Biak Basin (Papua Province, Eastern Indonesia). *Proceedings
532 Indonesian Petroleum Association Thirty-Seventh Annual Convention and Exhibition, IPA13-G-122*

533

534 Meyers, W.J., Lohmann, K.C., 1985. Isotope geochemistry of regionally extensive calcite cement
535 zones and marine components in Mississippian limestones, New Mexico. In: Schneidermann, N.,
536 Harris, P.M. (Eds.) Carbonate Cements. SEPM Special Publication 36, 223–239.

537

538 Milton, D. J., 1973. Water and processes of degradation in the Martian landscape. *Journal of*
539 *Geophysical Research* 78, 4037-4047.

540

541 Moore, C.H., Wade, W.J., 2013. Carbonate reservoirs: porosity and diagenesis in a sequence
542 stratigraphic framework 2nd Edition. Elsevier, Amsterdam.

543

544 Niemann, J.C., Read, J.F., 1987. Regional cementation from unconformity-recharged aquifer and
545 burial fluids, Mississippian Newman Limestone, Kentucky. *AAPG Bulletin* 58, 688–705.

546

547 Orange, D.L., Anderson, R.S., Breen, N., 1994. Regular submarine canyon spacing in the submarine
548 environment: the link between hydrology and geomorphology. *GSA Today* 4,36–39.

549

550 Orange, D.L., Breen, N.A., 1992. The effects of fluid escape on accretionary wedges 2. Seepage force,
551 slope failure, headless submarine canyons, and vents. *Journal of Geophysical Research: Solid Earth*,
552 97(B6), 9277-9295.

553

554 Pairault, A.A., Hall, R., Elders, C.F., 2003. Structural Styles and Tectonic Evolution of the Seram
555 Trough, Indonesia. *Marine and Petroleum Geology* 20, 1141–1160.

556

557 Paull, C.K., Spiess, F.N., Curray, J.R., Twichell, D.C., 1990. Origin of Florida Canyon and the role of
558 spring sapping on the formation of submarine box canyons. *Geological Society of America Bulletin*,
559 102(4), 502-515.

560

561 Paull, C.K., Neumann, A.C., 1987. Continental margin brine seeps: Their geological consequences.
562 *Geology* 15, 545-548.
563

564 Person, M., Dugan, B., Swenson, J.B., Urbano, L., Stott, C., Taylor, J., Willett, M., 2003. Pleistocene
565 hydrogeology of the Atlantic continental shelf, New England. *GSA Bulletin* 115, 1324–1343.
566

567 Quinn, T.M., 1991. Meteoric diagenesis of Plio-Pleistocene limestones at Enewetak atoll. *Journal of*
568 *Sedimentary Research* 61(5), 681-703.
569

570 Redmond, J.L., Koesoemadinata, R.P., 1976. Walio oil field and the Miocene carbonates of Salawati
571 basin, Irian, Jaya, Indonesia. *Proceedings Indonesian Petroleum Association, 5th Annual Convention*
572 *and Exhibition, Jakarta, 41-57.*
573

574 Robb, J.M., 1984. Spring sapping on the lower continental slope, offshore New Jersey. *Geology* 12,
575 278-282
576

577 Robb, J.M., 1990. *Groundwater processes in the submarine environment: Groundwater*
578 *Geomorphology: The Role of Subsurface Water in Earth-Surface Processes and Landforms.*
579 *Geological Society of America Special Paper* 252, 267-282.
580

581 Sangrey, D.A., 1977. Marine geotechnology: state-of-the-art. *Marine Geotechnology* 2, 45-80.
582

583 Scholle, P. A., Ulmer-Scholle, D. S., 2003. *A Color Guide to the Petrography of Carbonate Rocks:*
584 *Grains, textures, porosity, diagenesis. American Association of Petroleum Geologists Memoir* 77,
585 *Tulsa, OK*
586

587 Shackleton, N.J., Kennett, J.P., 1975. Palaeotemperature history of the Cenozoic and the interior of
588 Atlantic Glaciation: oxygen and carbon isotope analyses in DSDP sites 277, 279 and 281. Initial
589 Report DSDP 29, 743-753.

590

591 Small, R. J., 1965. The role of spring sapping in the formation of Chalk escarpment valleys,
592 Southampton Research Series in Geography 1, 3-29.

593

594 Spakman, W., Hall, R. 2010. Surface deformation and slab–mantle interaction during Banda arc
595 subduction rollback. *Nature Geoscience* 3, 562 – 566.

596

597 Tucker, M.E., Wright, V.P., 1990. *Carbonate sedimentology*. Blackwell Science, UK.

598

599 Wu, Y., Chafetz, H.S., 2002. Stable isotopic signature of a palaeoaquifer, mississippian Alamogordo
600 Member limestones, sacramento mountains, New Mexico, USA. *Sedimentology* 49(2), 227-235.

601

602 Yun, J.W, Orange, D.L., Field, M.E., 1999. Subsurface gas offshore of northern California and its link
603 to submarine geomorphology. *Marine Geology* 154, 357-368.